Preprints of the 21st IFAC World Congress (Virtual)
Berlin, Germany, July 12-17, 2020

A Backstepping-based observer for estimation of thermoacoustic oscillations in a Rijke tube with in-domain measurements

Gustavo Artur de Andrade * **Rafael Vazquez** **

* *Department of Automation and Systems, Universidade Federal de Santa Catarina, 88040-900, Florianópolis, SC, Brazil (e-mail: gustavo.artur@ufsc.br)*
** *Department of Aerospace Engineering, Universidad de Sevilla, Camino de los Descubrimientos, s.n.,41092 Sevilla, Spain (e-mail: rvazquez1@us.es)*

Abstract: This paper presents an observer design for estimation of thermoacoustic instabilities in a Rijke tube. To study this problem, we consider that the acoustic dynamics is represented by the wave equation with a point source term representing the heat release. In turn, the heat release dynamics is given by a first-order ordinary differential equation (ODEs). The observer, whose design is based on the backstepping methodology, relies on measurements of acoustic pressure and velocity at an arbitrary point of the domain. The design employs a folding transformation (with two folds) around the measurements and the heat release point, allowing to write the system into a form with more states but boundary measurements and ODE couplings. Then, we formulate a well-posed and invertible integral transformation with both triangular and full terms that maps the observer error dynamics into an exponentially stable target system. The theoretical results were tested through numerical simulations in order to show the effectiveness of the design.

Keywords: Backstepping, Rijke tube, Partial differential equations, Thermoacoustic instabilities, Observer design.

1. INTRODUCTION

The thermoacoustic phenomenon is described by high levels of sound produced due to the feedback between heat release rate fluctuations and acoustic pressure fluctuations in confined spaces. In some applications these oscillations are important to the successful operation of the system. However, in most cases this phenomenon remains a serious problem. Examples are steam and gas turbines, industrial burners, and jet and ramjet engines. In such applications, thermoacoustic instabilities are undesirable due to vibrations resulting in mechanical failures, high levels of acoustic noise, high burn rates, and component melting (Annaswamy and Ghoniem, 1995). Moreover, suppressing these oscillations is essential to achieve higher efficiencies and increasing the performance of the system.

Thermoacoustic instabilities are also observed in simpler devices, such as the Rijke tube benchmark, where the phenomenon can be reproduced without the presence of a combustion process. This makes the modeling and system analysis more tractable while still representing, with significant accuracy, combustion instabilities.

In this context, several researchers have focused on the modeling and control problem of the Rijke tube, with Heckl (1988) being one of the first to consider the open-loop stability analysis and control design. Recent results, such as Olgac et al. (2014); Epperlein et al. (2015), have focused in the distributed nature of the system with a frequency domain approach. Delayed feedback PI controllers were proposed in Zalluhoglu et al. (2016). Port-Hamiltonian control methods have also been recently used in Vincent et al. (2019).

In de Andrade et al. (2018b), we have applied the infinite dimensional backstepping methodology to design a state feedback control law to mitigate thermoacoustic oscillations in the Rijke tube, using the concept of *folding* (Vazquez and Krstic, 2016; Chen et al., 2019a,b). The idea of folding transformations is to separate the PDEs into different spatial domains, and impose compatibility conditions on the resulting internal boundaries. This technique admits a design parameter (named the folding point) which, in our case, was chosen as the ODE coupling point in order to displace it to the boundary conditions. This allowed us to map the system into an equivalent one with more states, but boundary couplings, to which backstepping could be applied.

To extend this result to an output control law, a backstepping boundary observer was developed in de Andrade et al. (2018a). However, in this previous work we only considered boundary acoustic pressure measurements, which may be problematic because an open end tube typically induces acoustic pressure nodes at the boundaries (Morse

⋆ This work was funded by the Spanish Ministerio de Ciencia, Innovación y Universidades under grant PGC2018-100680-B-C21

and Ingard, 1968). Consequently, sensors installed in those points may give poor measurements.

This paper is an extension of our previous work (de Andrade et al., 2018a), where in-domain pressure and velocity measurements are considered in the backstepping observer design. The same idea of folding is now applied, but now with a *double fold*, with the second folding done at the in-domain measurement point in order to translate it to the boundary. This allows us to map the system into an equivalent one with even more states, but boundary measurements and couplings. As before, the resulting equations have a non-strict-feedback form which restricts the choice of the backstepping transformation and target system. This issue is tackled, as in (de Andrade et al., 2018a), by formulating a well-posed and invertible integral transformation with triangular and full terms that maps the plant into an exponentially stable target system. The resulting target system is exponentially stable at the zero equilibrium point of the error dynamics. In addition, the observer gains are computed by an explicit expression depending on the kernels, which in turn are exactly calculated from the kernel equations. These theoretical results are tested through numerical simulations in order to show the effectiveness of the design.

The paper is organized as follows. A brief presentation of the linear mathematical model of the phenomenon of thermoacoustic instabilities in the Rijke tube, as well as the state estimation problem and folding transformation are described are described in Section 2. The backstepping observer design is detailed in Section 3. The result is summarized in Section 4 where we state the theorem proved in this work. Simulation results are presented in Section 5. Finally, the conclusions and future works are highlighted in Section 6.

2. IN-DOMAIN STATE ESTIMATION OF THERMOACOUSTIC INSTABILITIES OF THE LINEARIZED RIJKE TUBE

2.1 Statement of the problem

The linearized model of the Rijke tube can be captured by the following equations (Epperlein et al., 2015):

$$\partial_t v(t,\, x) + \frac{1}{\overline{\rho}}\partial_x P(t,\, x) = 0, \tag{1}$$

$$\partial_t P(t,\, x) + \gamma \overline{P}\partial_x v(t,\, x) = \frac{\overline{\gamma}}{A}\delta(x - x_0)Q(t), \tag{2}$$

$$\tau_{hr}\dot{Q}(t) + Q(t) = f'(\overline{v})(T_w - \overline{T}_{gas})v(t,\, x_0), \tag{3}$$

where $t \in [0, +\infty)$ is the time [s], $x \in [0, L]$ is the space [m], and δ is the Dirac delta distribution [1/m]. The distributed state v stands for the velocity fluctuations [m/s], and P for the pressure fluctuations [Pa]. The steady-state velocity [m/s], density [kg/m^3] and pressure [Pa] are given by $\overline{v}$, $\overline{\rho}$ and $\overline{P}$, respectively. The tube cross-section area [m^2] is given by A, the heat capacity ration is given by $\gamma = \frac{C_P}{C_v}$, where C_p and C_v are the specific heat capacity [J/(kg K)] at constant pressure and volume conditions respectively, x_0 is the location of the heat release source [m], and Q is the heat power release [W]. $\tau_{hr} > 0$ is the heat release time constant [s], $f(\overline{v}) = l_w(\kappa + \kappa_v\sqrt{|\overline{v}|}) > 0$ is the heat power transfer, whereas l_w is the wire length [m], κ is the fluid thermal conductivity [W/(m K)], κ_v is an empirical constant, and $\bar{\gamma} = \gamma - 1 > 0$. Finally, T_w and $\overline{T}_{gas}$, with $T_w - T_{gas} > 0$, stand for the wire and gas temperature [K], respectively.

System (1)-(3) is subject to the following boundary conditions:

$$P(t,\, 0) = -Z_0 v(t,\, 0) + U(t), \qquad P(t,\, L) = Z_L v(t,\, L), \tag{4}$$

where $Z_L \neq 0$ and $Z_0 \neq 0$ are reflection losses [Pa s/m] and U is the control variable [Pa].

The initial condition of (1)-(4) is given by

$$v(0,\, x) = v_0(x), \qquad P(0,\, x) = P_0(x), \qquad Q(0) = Q_0,$$

with $Q_0 \in \mathbb{R}$ and $v_0,\, P_0 \in \mathcal{L}_2([0,\, L])$.

The *in-domain observer problem* is then the problem to design an observer that provides accurate online estimates of both the finite-dimensional state Q and the distributed state variables P and v. The observer must only make use of the system input U (although closed-loop control is not investigated in this paper) and outputs

$$y_1(t) = P(t,\, x_m), \qquad y_2(t) = v(t,\, x_m), \tag{5}$$

with $x_m \in (0, L)$.

Remark 1. In de Andrade et al. (2018a), the observer design is investigated for (1)-(4) with measurements of $P(t,\, L)$. The results considered here are more general than the one in de Andrade et al. (2018a), even though more measurements are considered. More importantly, the resulting estimator is expected to be more reliable, as the point x_m can be chosen such that pressure nodes (which can distort the measure) are avoided.

2.2 Characteristic coordinates

Consider the following change of coordinates:

$$P(t,\, x) = \frac{1}{2}(R_1(t,\, x) + R_2(t,\, x)), \tag{6}$$

$$v(t,\, x) = \frac{1}{2\sqrt{\gamma\overline{P}\overline{\rho}}}(R_1(t,\, x) - R_2(t,\, x)). \tag{7}$$

With this change of coordinates, the system (1)-(4) can be rewritten as 2×2 transport PDEs convecting in opposite directions with a point source term:

$$\partial_t R_1(t,\, x) + c\partial_x R_1(t,\, x) = \frac{\bar{\gamma}}{A}\delta(x - x_0)Q(t), \tag{8}$$

$$\partial_t R_2(t,\, x) - c\partial_x R_2(t,\, x) = \frac{\bar{\gamma}}{A}\delta(x - x_0)Q(t), \tag{9}$$

$$\tau_{hr}\dot{Q}(t) = -Q(t) + q(R_1^-(t,\, x_0) - R_2^+(t,\, x_0)), \tag{10}$$

where $c = \sqrt{\gamma\frac{\overline{P}}{\overline{\rho}}}$ is the speed of sound [m/s], and $q = \frac{f'(\overline{v})(T_w - T_{gas})}{2\sqrt{\gamma\overline{P}\overline{\rho}}} > 0n.$

In addition, the boundary conditions (4) are rewritten to

$$R_1(t,0) = k_0 R_2(t,0) + 2U(t), \;\; R_2(t,L) = k_L R_1(t,L), \tag{11}$$

with $k_L = \frac{Z_L - \bar{\rho}c}{Z_L + \bar{\rho}c}$ and $k_0 = \frac{Z_0 - \bar{\rho}c}{Z_L + \bar{\rho}c}$.

Finally, using (6)-(7) in (5) we obtain the following outputs:

$$y_1(t) = \frac{1}{2}\left(R_1(t,x_m) + R_2(t,x_m)\right), \tag{12}$$

$$y_2(t) = \frac{1}{2\sqrt{\gamma\overline{P}\overline{\rho}}}\left(R_1(t,x_m) - R_2(t,x_m)\right). \tag{13}$$

2.3 Folding transformation

In this section we propose a transformation to remove the Dirac delta distribution in (8)-(9) and to translate the measurements (12)-(13) to the boundary conditions. Importantly, the transformation must be separated into two different cases: (i) for $x_m > x_0$ and; (ii) for $x_m < x_0$. For sake of brevity, only the first case will be developed in this paper. The other case can be obtained in a similar fashion.

Let x_0 and x_m be the points to fold the system (8)-(11). We then consider the following piecewise definition of R_1 and R_2:

$$R_1(t,x) = \begin{cases} \alpha_1(t,x),\ x \in [0,x_0], \\ \beta_2(t,x),\ x \in [x_0,x_m], \\ \alpha_3(t,x),\ x \in [x_m,L], \end{cases} \tag{14}$$

$$R_2(t,x) = \begin{cases} \beta_1(t,x),\ x \in [0,x_0], \\ \alpha_2(t,x),\ x \in [x_0,x_m], \\ \beta_3(t,x),\ x \in [x_m,L], \end{cases} \tag{15}$$

and define the following piecewise spatial transformation in z:

$$z = \begin{cases} \dfrac{x}{x_0}, & x \in [0,x_0], \\ \dfrac{L-x}{L-x_0}, & x \in [x_0,x_m], \\ \dfrac{x-x_m}{L-x_m}, & x \in [x_m,L]. \end{cases} \tag{16}$$

This set of scaling and folding transformations allows us to map the system (8)-(11) into the following matrix system:

$$\partial_t\alpha(t,z) + \Lambda\partial_z\alpha(t,z) = 0, \tag{17}$$

$$\partial_t\beta(t,z) - \Lambda\partial_z\beta(t,z) = 0, \tag{18}$$

$$\tau_{hr}\dot{Q}(t) + Q(t) = q(\alpha_1(t,1) - \alpha_2(t,1)), \tag{19}$$

where

$$\alpha = (\alpha_1,\ \alpha_2,\ \alpha_3), \qquad \beta = (\beta_1,\ \beta_2,\ \beta_3),$$
$$\Lambda = \mathrm{diag}(\lambda_1,\ \lambda_2,\ \lambda_3),$$

with $\lambda_1 = c/x_0$, $\lambda_2 = c/(x_m - x_0)$, and $\lambda_3 = c/(L - x_m)$.

Applying (14)-(16) into (11), we obtain the following boundary conditions:

$$\alpha(t,\,0) = N_i\beta(t,\,0) + N_uU(t), \tag{20}$$

$$\beta(t,\,1) = N_f\alpha(t,\,1) + N_qQ(t), \tag{21}$$

where

$$N_i = \begin{pmatrix} k_0 & 0 & 0 \\ 0 & 0 & 1 \\ 0 & 1 & 0 \end{pmatrix}, \qquad N_u = \begin{pmatrix} 2 \\ 0 \\ 0 \end{pmatrix},$$

$$N_f = \begin{pmatrix} 0 & 1 & 0 \\ 1 & 0 & 0 \\ 0 & 0 & k_L \end{pmatrix}, \qquad N_q = \begin{pmatrix} c_1 \\ c_1 \\ 0 \end{pmatrix}.$$

Finally, (12)-(13) are rewritten to

$$\beta_2(t,\,0) = y_1(t) + \sqrt{\gamma\overline{P}\overline{\rho}}\,y_2(t), \tag{22}$$

$$\beta_3(t,\,0) = y_1(t) - \sqrt{\gamma\overline{P}\overline{\rho}}\,y_2(t). \tag{23}$$

In this framework, the in-domain observer problem can be restated as the boundary observer problem (17)-(21) with measurements (22)-(23). Our objective now is to design an state observer for these equations.

3. OBSERVER DESIGN AND ERROR DYNAMICS ANALYSIS

3.1 Observer design

Let $\hat{\alpha}_i$ and $\hat{\beta}_i$, for $i \in \{1,\dots,3\}$, and $\hat{Q}$ be the estimated states. We design the observer as a copy of (17)-(21) plus output injection terms:

$$\partial_t\hat{\alpha}(t,z) + \Lambda\partial_z\hat{\alpha}(t,z) = -p^+(z)\tilde{y}_{\beta_2}(t), \tag{24}$$

$$\partial_t\hat{\beta}(t,z) - \Lambda\partial_z\hat{\beta}(t,z) = -p^-(z)\tilde{y}_{\beta_2}(t), \tag{25}$$

$$\tau_{hr}\dot{\hat{Q}}(t) + \hat{Q}(t) = q(\hat{\alpha}_1(t,\,1) - \hat{\alpha}_2(t,\,1)) - p_Q\tilde{y}_{\beta_2}(t), \tag{26}$$

with boundary conditions

$$\hat{\alpha}(t,0) = N_i\hat{\beta}(t,0) + N_uU(t) + p_{bc}\tilde{y}(t), \tag{27}$$

$$\hat{\beta}(t,\,1) = N_f\hat{\alpha}(t,1), + N_q\hat{Q}(t) \tag{28}$$

In (24)-(28), p^+, p^-, p_Q and p_{bc} are the gains to be found, with

$$p^+ = (p_1^+,\ 0,\ 0), \qquad p^- = (p_1^-,\ p_2^-,\ 0),$$

$$p_bc = \begin{pmatrix} p_{bc}^1 & p_{bc}^2 \\ p_{bc}^3 & p_{bc}^4 \\ p_{bc}^5 & p_{bc}^6 \end{pmatrix}, \qquad \tilde{y} = (\tilde{y}_{\beta_2},\,\tilde{y}_{\beta_3}),$$

and

$$\tilde{y}_{\beta_2}(t) = \beta_2(t,0) - \hat{\beta}_2(t,\,0) = \tilde{\beta}_2(t,\,0),$$
$$\tilde{y}_{\beta_3}(t) = \beta_3(t,0) - \hat{\beta}_3(t,\,0) = \tilde{\beta}_3(t,\,0).$$

Remark 2. Only the output y_{β_2} is injected in equations (24)-(26). We have used two in-domain point measurements to compute the states in the characteristic coordinates from both sensors, which would not be possible if only one state were measured.

3.2 Target system

Define the estimation error as $\tilde{\alpha}_i = \alpha_i - \hat{\alpha}_i$, $\tilde{\beta}_i = \beta_i - \hat{\beta}_i$, for $i \in \{1,\dots,3\}$, and $\tilde{Q} = Q - \hat{Q}$. Then, using (17)-(21) and (24)-(28), we obtain the following error dynamics:

$$\partial_t\tilde{\alpha}(t,z) + \Lambda\partial_z\tilde{u}(t,z) = p^+(z)\tilde{y}_{\beta_2}(t), \tag{29}$$

$$\partial_t\tilde{\beta}(t,z) - \Lambda\partial_z\tilde{\beta}(t,z) = p^-(z)\tilde{y}_{\beta_2}(t), \tag{30}$$

$$\tau_{hr}\dot{\tilde{Q}}(t) + \tilde{Q}(t) = q(\tilde{\alpha}_1(t,\,1) - \tilde{\alpha}_2(t,\,1)) + p_Q\tilde{y}_{\beta_2}(t), \tag{31}$$

with boundary conditions

$$\tilde{\alpha}(t,\,0) = N_i\tilde{\beta}(t,\,0) - p_{bc}\tilde{y}(t), \tag{32}$$

$$\tilde{\beta}(t,\,1) = N_f\tilde{\alpha}(t,\,1) + N_q\tilde{Q}(t), \tag{33}$$

Note that the error dynamics behavior is similar to the open-loop system (17)-(21), which is potentially unstable. Therefore, we must design the observer gains in order to make (29)-(33) exponentially stable. In particular, we seek to map (29)-(33) into the following target system:

$$\partial_t\breve{\alpha}(t,z) + \Lambda\partial_z\breve{\alpha}(t,z) = 0, \tag{34}$$

$$\partial_t\breve{\beta}(t,z) - \Lambda\partial_z\breve{\beta}(t,z) = 0, \tag{35}$$

$$\tau_{hr}\dot{\breve{Q}}(t) + (qc_1 + 1)\breve{Q}(t) = -q\breve{\alpha}_2(t,\,1), \tag{36}$$

with boundary conditions

$$\check{\alpha}_1(t,\,0) = k_0\check{\beta}_1(t,\,0), \tag{37}$$
$$\check{\alpha}_2(t,\,0) = 0, \tag{38}$$
$$\check{\alpha}_3(t,\,0) = 0, \tag{39}$$
$$\check{\beta}(t,\,1) = N_f\check{\alpha}(t,\,1) + N_q\check{Q}(t). \tag{40}$$

Lemma 1. Consider system (34)-(40) with initial condition $(\check{\alpha}_{1,0},\,\alpha_{2,\,0},\,\alpha_{3,\,0},\,\check{\beta}_{1,0},\,\check{\beta}_{2,0},\,\check{\beta}_{3,0},\,\check{Q}) \in (\mathcal{L}_2(0,\,1))^6 \times \mathbb{R}$. Then, the zero equilibrium point of (34)-(40) exponentially stable in the $\mathcal{L}_2$ sense.

The proof of Lemma 1 can be constructed by considering the explicit solution of (34)-(40).

3.3 Backstepping transformation

To map the error dynamics (29)-(33) into the target system (34)-(33), we use the following transformation (de Andrade et al., 2018a):

$$\tilde{Q}(t) = \check{Q}(t) + \int_0^1 K_Q(\xi)\check{\beta}_2(t,\xi)d\xi, \tag{41}$$
$$\tilde{\alpha}_1(t,z) = \check{\alpha}_1(t,z) + \int_0^1 K_1(z,\xi)\check{\beta}_2(t,\xi)d\xi, \tag{42}$$
$$\tilde{\beta}_1(t,z) = \check{\beta}_1(t,z) + \int_0^1 S_1(z,\xi)\check{\beta}_2(t,\xi)d\xi, \tag{43}$$
$$\tilde{\beta}_2(t,z) = \check{\beta}_2(t,z) + \int_0^z S_2(z,\xi)\check{\beta}_2(t,\xi)d\xi. \tag{44}$$

Introducing (41)-(44) into (29)-(33), applying (34)-(36), integrating by parts and substituting the boundary conditions (37)-(40), we obtain that (41)-(44) maps (29)-(33) into (34)-(40) if and only if the kernels satisfy the following equations:

$$\lambda_2\partial_\xi K_1(z,\xi) - \lambda_1\partial_z K_1(z,\xi) = 0, \tag{45}$$
$$\lambda_2\partial_\xi S_1(z,\xi) + \lambda_1\partial_z S_1(z,\xi) = 0, \tag{46}$$
$$\partial_\xi S_2(z,\xi) + \partial_z S_2(z,\xi) = 0, \tag{47}$$
$$\tau_{hr}\lambda_2 K_Q'(\xi) - K_Q(\xi) = -qK_1(1,\,\xi), \tag{48}$$

with boundary conditions

$$K_1(z,\,1) = S_1(z,\,1) = 0, \;\; K_Q(1) = \frac{q}{\tau_{hr}\lambda_2}, \tag{49}$$

In addition, the observer gains are given by

$$p_1^+(z) = -\lambda_2 K_1(z,0), \tag{50}$$
$$p_i^-(z) = -\lambda_2 S_i(z,0), \qquad i \in \{1,\,2\}, \tag{51}$$
$$p_Q = -\tau_{hr}\lambda_2 K_Q(0). \tag{52}$$
$$p_{bc} = \begin{pmatrix} 0 & 0 \\ 0 & 1 \\ 1 & 0 \end{pmatrix}. \tag{53}$$

Besides, substituting (42)-(44) into the boundary conditions (32)-(33), we get that

$$K_1(0,\,\xi) = k_0 S_1(0,\,\xi), \tag{54}$$
$$S_1(1,\,\xi) = c_1 K_Q(\xi), \tag{55}$$
$$S_2(1,\,\xi) = K_1(1,\,\xi) + c_1 K_Q(\xi), \tag{56}$$

3.4 Well-posedness of the kernel equations and invertibility of the backstepping transformation

Unique solution of the kernel equations

To find the unique solution of (45)-(49), (54)-(56) we take into account the Riemann invariant property of these equations and use the method of characteristics, which allows us to find an explicit solution.

Solution of the K_1 kernel. Following the characteristic lines of (45), taking into account that K_1 is constant along the characteristics and applying boundary conditions (49) and (54) we get that

$$K_1(z,\,\xi) = \begin{cases} 0, & \text{if } \dfrac{\lambda_1}{\lambda_2}\xi + z \geq \dfrac{\lambda_1}{\lambda_2}, \\ k_0 S_1\left(0,\,\xi + \dfrac{\lambda_2}{\lambda_1}z\right), & \text{otherwise.} \end{cases} \tag{57}$$

Solution of the S_1 kernel. Integrating (46) along its characteristic lines and plugging boundary conditions (49)-(55)

$$S_1(z,\,\xi) = \begin{cases} 0, & \dfrac{\lambda_1}{\lambda_2}(\xi - 1) \geq z - 1, \\ c_1 K_Q\left(\xi - \dfrac{\lambda_2}{\lambda_1}(z-1)\right), & \text{otherwise.} \end{cases} \tag{58}$$

Solution of the S_2 kernel. Applying the method of characteristics into (47) and considering the boundary condition (56), we obtain the following explicit solution for S_2:

$$S_2(z,\,\xi) = K_1(1,\,1-z+\xi) + c_1 K_Q(1-z+\xi), \tag{59}$$

for all $z \in [0,\,1]$ and $\xi \in [0,\,1]$.

Solution of the K_Q kernel. The explicit expressions of (57) allows us to rewrite (48) as a delay differential equation with boundary condition given by (49) (it can be solved backwards from $\xi = 1$ to $\xi = 0$). Indeed, considering (57), we rewrite (48) to:

for $\xi \in [1 - 2\frac{\lambda_2}{\lambda_1},\,1]$:

$$\tau_{hr}\lambda_2 K_Q'(\xi) - K_Q(\xi) = 0, \tag{60}$$

for $\xi \in [0,\,1 - 2\frac{\lambda_2}{\lambda_1}]$:

$$\tau_{hr}\lambda_2 K_Q'(\xi) - K_Q(\xi) = -qk_0c_1K_Q\left(\xi + 2\frac{\lambda_2}{\lambda_1}\right). \tag{61}$$

Thus, the corresponding solution can be constructed by using the *method of steps* (de Andrade et al., 2018b,a). This result is summarized in the following lemma:

Lemma 2. Consider the following delay differential equation:

$$\tau_{hr}K_Q'(\xi) - K_Q(\xi) = -qk_0c_1K_Q\left(\xi + 2\frac{\lambda_2}{\lambda_1}\right), \tag{62}$$
$$K_Q(1) = \frac{q}{\tau_{hr}\lambda_2}, \tag{63}$$
$$K_Q(\theta) = 0, \quad \theta > 1. \tag{64}$$

Then, there exists a piecewise unique function $K_Q(\xi)$ on $\xi \in [0,\,1]$ that is absolutely continuous, satisfies (62)-(64) almost everywhere and is given by

$$K_Q(\xi) = \begin{cases} K_{Q,\,0}(\xi), \text{ if } \xi \in \Omega_0, \\ \vdots \\ K_{Q,\,n}(\xi), \text{ if } \xi \in \Omega_n, \end{cases}$$

where

$$\Omega_k \quad = \quad \left\{\xi \in [0,\,1] : 1 - \frac{2^{k+1}\lambda_2}{\lambda_1} \leq \xi \leq 1 - \frac{2^k\lambda_2}{\lambda_1}\right\}.$$

In addition, the explicit expression of $K_{Q,0}(\xi)$ is given by

$$K_Q(\xi) = -\frac{q}{\tau_{hr}\lambda_2} \mathrm{e}^{\frac{1}{\tau_{hr}\lambda_2}(\xi-1)},$$

and for $n \geq 1$ we have

$$K_Q(\xi) = K_{Q,\,n}(\xi) = \left[\mathrm{e}^{\frac{2^k}{\tau_{hr}\lambda_1}} K_{Q,\,k-1}\left(1 - \frac{2^k\lambda_2}{\lambda_1}\right) + \right.$$

$$\left. \frac{qk_0c_1}{\tau_{hr}\lambda_2} \int_{\xi}^{1-\frac{2^k\lambda_2}{\lambda_1}} \mathrm{e}^{-\frac{\theta-1}{\tau_{hr}\lambda_2}} K_{Q,\,k-1}\left(\theta + 2\frac{\lambda_2}{\lambda_1}\right) \right] \mathrm{e}^{\frac{1}{\tau_{hr}\lambda_2}(\xi-1)}.$$

Remark 3. The number of piece in the solution of the K_Q depends on the distance between the location of the heat release and the measurement point. In particular, the number of pieces is given by the greater natural number n such that $1 - 2^n\frac{\lambda_2}{\lambda_1} > 0$, i.e., $\frac{1}{2^n} > \frac{x_0}{x_m - x_0}$.

With the above results we have proved the following proposition:

Proposition 1. The kernel equations (45)-(49), (54)-(56) have a unique solution in $(\mathcal{L}_\infty(0,\,1))^6 \times \mathbb{R}$.

Invertibility of the backstepping transformation

Next, we show the invertibility of the backstepping transformation (41)-(44). Proving such property is crucial to ensure that the gains (50)-(51) map $(\tilde{\alpha},\,\tilde{\beta},\,\tilde{Q})$ into $(\check{\alpha},\,\check{\beta},\,\check{Q})$.

First, note that (44) is a Volterra integral equation of the second kind. Then, by Proposition 1 we know that $S_1(z,\,\xi)$ is bounded (with a finite number of *jump* discontinuities), which in turn means that (44) is invertible, i.e., there exists an unique kernel L_2 such that

$$\check{\beta}_2(t,\,z) = \tilde{\beta}_2(t,\,z) + \int_0^z L_2(z,\,\xi)\tilde{\beta}_2(t,\,\xi)d\xi.$$

Noticing the cascade structure (41)-(43) and plugging the above equation for $\check{\beta}_2$ into (41)-(43), an inverse transformation composed of both Volterra and full integral terms is computed. Therefore, (41)-(44) are invertible transformations.

4. MAIN RESULT

The main result of this paper is summarized in the following theorem:

Theorem 1. Consider system (29)-(33) with initial condition $(\tilde{\alpha},\,\tilde{\beta},\,\tilde{Q}) \in (\mathcal{L}_2(0,1))^6 \times \mathbb{R}$ and gains p_i^+, p_i^-, for $i \in \{1,\ldots,3\}$, p_Q and p_{bc} defined by (50)-(52), respectively. Then, under the assumption that $q,\,c_1 > 0$, the zero equilibrium point of (29)-(33) is exponentially stable in the $\mathcal{L}_2$ sense, i.e., the observer estimates converge to the values of the states.

Using the results developed in the previous sections, this theorem can be proved with standard arguments (Krstic and Smyshlayeav, 2008).

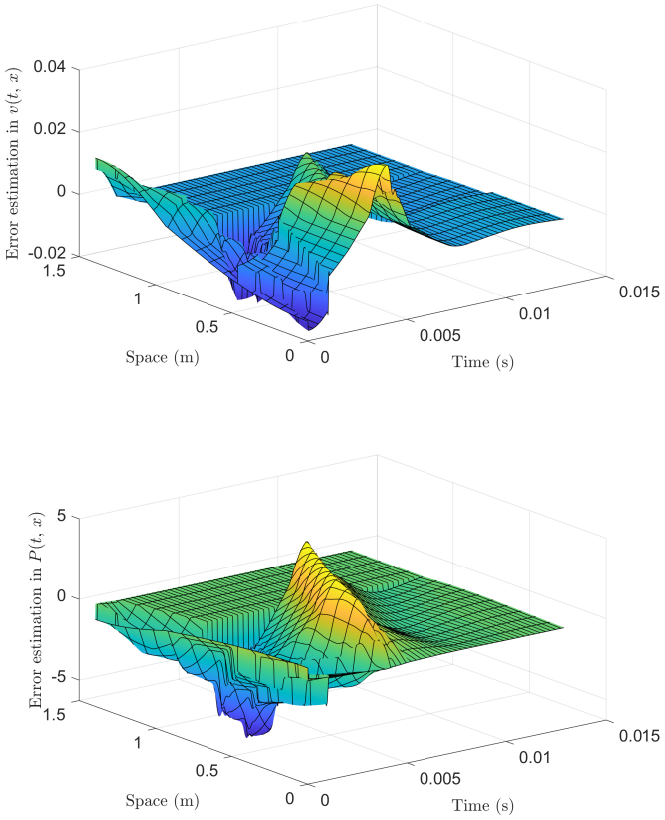

Fig. 1. Estimation error in $v(t,\,x)$ and $P(t,\,x)$ as a function of time and space.

5. SIMULATION RESULTS

This section shows the simulation results, where (17)-(21) was used as virtual plant, obtained when using the proposed observer design (24)-(28) with the gains (50)-(53). These equations were numerically solved using the HPDE solver for Matlab (Shampine, 2015) with a two-step variant of the Lax-Friedrichs method. In order to ensure the numerical stability, the time and space steps were chosen such that the Courant-Friedrichs-Lewy conditionn is satisfied. Finally, the parameter values for the simulation scenario were borrowed from de Andrade et al. (2018b,a) and are not detailed here due to lack of space. Importantly, we considered the location of the heat release as $x_0 = \frac{1}{4}L$ and the sensors measurement point as $x_m = \frac{3}{4}L$.

Figure 1 depicts the observer error dynamics (see (29)-(33)) obtained from the simulation scenario. As can be seen, the error exponentially converges to zero as $t \to \infty$, as stated in Theorem 1. Furthermore, we can see in this figure that the convergence is slow for the upstream part of the tube, i.e., for $x \in [0,\,x_0]$. This is in agreement with the choice of the target system proposed in Section 3.2, since for all $t \geq 2/\lambda_3 + 1/\lambda_2$ we have that $\check{\alpha}_3(t,\,z) = \check{\alpha}_2(t,\,z) = \check{\beta}_3(t,\,z) = 0$, which corresponds to the characteristic coordinates of P and v (see equations (6)-(7), (14)-(16)). The estimation error in the heat power release is depicted in Figure 2. Note that $\hat{Q}$ converges to the real value after the initial transient.

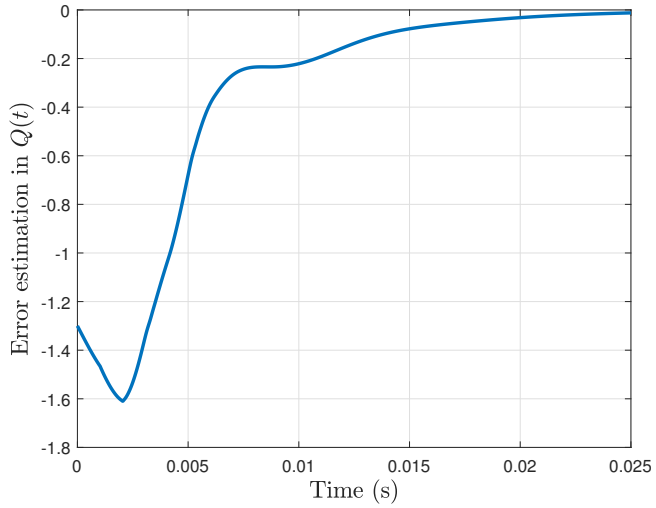

Fig. 2. Estimation error in $Q(t)$ as a function of time.

6. CONCLUSIONS

This paper considers the state estimation of thermoacoustic instabilities of the linearized Rijke tube model with in-domain measurements. The proposed method uses a double folding transformation to rewrite the estimation problem as a boundary state estimation framework. Then, a Luenberger-type observer was introduced and the output injection gains were obtained by the backstepping method. The kernels of the backstepping transformation were solved analytically by the method of characteristics, which in turn allows us to obtain an explicit expression for the observer gains. In particular, the kernels are piecewise smooth and the number of pieces depends on the distance between the heat release location and the measurement point.

The result presented in this work generalizes our previous paper (de Andrade et al., 2018a), where only the case of boundary pressure measurements was investigated. In addition, it is more reliable from a practical point of view, since the designer can shift the location of the measurement point in order to avoid pressure nodes and to enable a trade-off between observer complexity and performance.

The proposed method is, to the best of our knowledge, the first result on observer design for a PDE-ODE system with in-domain measurements using the backstepping technique. This raises the question to extend the methodology for more general systems with in-domain point measurements. In particular future works will consider other PDE-ODE systems with a smaller number of measured states. Another direction of future works includes the robustness analysis of the proposed observer. From an application point of view, this is highly important, as the measurements usually are corrupted by noise or even the mathematical model suffers from uncertainties.

REFERENCES

Annaswamy, A.M. and Ghoniem, A. (1995). Active control in combustion systems. *IEEE Control Systems*, 15, 49–63.

Chen, S., Vazquez, R., and Krstic, M. (2019a). Bilateral boundary control design for a cascaded diffusion-ODE system coupled at an arbitrary interior point. *Automatica*, 96, 98–109.

Chen, S., Vazquez, R., and Krstic, M. (2019b). Folding bilateral backstepping output-feedback control design for an unstable parabolic PDE. *IEEE Transactions on Automatic Control*, 96, 98–109.

de Andrade, G.A., Vazquez, R., and Pagano, D.J. (2018a). Backstepping-based linear boundary observer for estimation of thermoacoustic instabilities in a Rijke tube. In *Proceedings of the 57th IEEE Conference on Decision and Control*, 2164–2169.

de Andrade, G.A., Vazquez, R., and Pagano, D.J. (2018b). Backstepping stabilization of a linearized ODE-PDE rijke tube model. *Automatica*, 96, 98–109.

Epperlein, J.P., Bamieh, B., and Astrom, J. (2015). Thermoacoustics and the Rijke tube: Experiments, identification and modeling. *Control Systems Magazine*, 35(2), 57–77.

Heckl, M.A. (1988). Active control of the noise from a Rijke tube. *Journal of Sound and Vibration*, 124(1), 117–133.

Krstic, M. and Smyshlayeav, A. (2008). *Boundary control of PDEs: a course on backstepping designs*. SIAM.

Lamare, P.O., Auriol, J., Di Meglio, F., and Aarsnes, U.J.F. (2018). Robust output regulation of 2×2 hyperbolic systems: Control law and input-to-state satability. In *Proceedings of the 57th IEEE American Control Conference*, 1732– 173.

Morse, P.M. and Ingard, K.U. (1968). *Theoretical acoustics*. McGraw-Hill Book Company.

Olgac, N., Zalluhoglu, U., and Kammer, A.S. (2014). Preddicting thermoacoustic instability: A novel analytical approach and its experimental validation. *Journal of Propulsion and Power*, 30(4), 1005–1015.

Shampine, L.F. (2015). Solving hyperbolic PDEs in MATLAB. *Applied Numerical Analysis and Computational Mathematics Journal*, 2, 346–358.

Vazquez, R. and Krstic, M. (2016). Bilateral boundary control of one-dimensional first- and second-order PDEs using infinite-dimensional backstepping. In *Proceedings of the 55th IEEE Conference on Decision and Control*, 537–542.

Vincent, B., Hudon, N., Lefèvre, L., and Dochain, D. (2019). Modelling of thermo-acoustic instabilities. In *Proceedings of the IFAC Workshop TFMST*, 35–40.

Zalluhoglu, U., Kammer, A.S., and Olgac, N. (2016). Delayed feedback control laws for Rijke tube thermoacoustic: Instability, synthesis, and experimental validation. *IEEE Transactions on Control Systems Technology*, 24(5), 1861–1868.